HAL
open science

On Material Removal Regimes for the Shaping of Glass Edges: Force Analysis, Surface Topography and Damage Mechanisms

Ibrahim Demirci, Sabeur Mezghani, Mohamed El Mansori

To cite this version:

Ibrahim Demirci, Sabeur Mezghani, Mohamed El Mansori. On Material Removal Regimes for the Shaping of Glass Edges: Force Analysis, Surface Topography and Damage Mechanisms. Tribology Letters, 2008, 30, pp.141-150. 10.1007/s11249-008-9320-7 . hal-00881200

HAL Id: hal-00881200

https://hal.science/hal-00881200v1

Submitted on 12 Nov 2013

HAL is a multi-disciplinary open access archive for the deposit and dissemination of scientific research documents, whether they are published or not. The documents may come from teaching and research institutions in France or abroad, or from public or private research centers.

L'archive ouverte pluridisciplinaire **HAL**, est destinée au dépôt et à la diffusion de documents scientifiques de niveau recherche, publiés ou non, émanant des établissements d'enseignement et de recherche français ou étrangers, des laboratoires publics ou privés.

On Material Removal Regimes for the Shaping of Glass Edges: Force Analysis, Surface Topography and Damage Mechanisms

I. Demirci · S. Mezghani · M. El Mansori

Abstract Glass shaping, which corresponds to the removal of the edges of a specimen, is the last finishing operation in glass manufacturing. This process has several functions on the final shaped glass including removing sharp edges, improving mechanical resistance, decreasing surface damage and giving it an aesthetical aspect. This article addresses the effects of working parameters, including grinding forces and consumed power, on surface edge finishing and damage mechanism induced during glass grinding. Microscopic observations and multi-scale analysis have also been conducted to investigate the surface edge characteristics. Experimental results show three damage regimes. The first (regime I) is a partial ductile regime with cutting action accompanied by chip formation. The second (regime II) is a crushing (or fragmentation) regime. The last (regime III) is also a partial ductile regime but by ploughing action with displaced material. The shaped surface obtained in the regime II has a better roughness than that obtained in regime I and III. However, regimes I and III include streaks and form defects which are not present in regime II. Similar to metallic materials, the evolution of force components show a linear relationship between normal and tangential forces. This implicates a constant average contact pressure and friction coefficient (μ) between the flat grains and the workpiece.

Keywords Grinding · Wear mechanism · Abrasive wear · Glass · Surface roughness

I. Demirci (✉) · S. Mezghani · M. El Mansori
LMPF (EA 4106) – ENSAM, Rue Saint Dominique, BP 508, Chalons-en-Champagne 51006, France
e-mail: ibrahim.demirci@ensam.fr

1 Introduction

Glass and glass-ceramics are usually machined by grinding process with either silicon carbide (SiC) or diamond grinding wheels. The last operation practiced for glass manufacturing is glass shaping, which corresponds to the machining of the edge of specimen. This process has several functions:

- To remove the sharp edges and the irregularities for handling without risk;
- To improve the mechanical resistance of the glass joint by removing the surface damage. Indeed the resistance of glasses (and brittle material in general) usually depends on surface damages which grow dramatically until complete rupture of the material;
- To give the glass joints a particular fixing function and an aesthetic aspect.

Material removal by abrasion in brittle materials is still not fully understood. The process is complicated in grinding due to the large number of the abrasive grains that interact with the workpiece surface. Further complications result from the random shape and geometry of the grain arrangement on the grinding wheel.

Investigation performed in the 1970s [1–3] showed that glass, a brittle material, might flow during grinding under certain conditions. Some investigations [2, 3] concluded that flow occurs when the surface temperature reaches the softening temperature of the glasses. However, Bridgman and Simon [4] showed that under high hydrostatic stress, glass would flow even at room temperature. More recently, a close attention was paid to both finishing and super finishing of optical glasses, especially for investigation of obtaining flow. New grinding techniques were developed to study this behaviour. Venkatesh et al. [5] developed two novel techniques to study the formation of streaked

surfaces in a ductile mode during diamond grinding of optical lens. The first was aspheric grinding and the second high speed grinding. With these techniques, two different streaks were obtained: one with cutting action accompanied by chip formation and another by ploughing action with displaced material. Sun et al. [6] tested different methods such as parallel and perpendicular grinding, and they indicated the possibility of obtaining a ductile streak.

It was also shown that the nature of bond and grain play an important role on surface finish performances and on obtaining flow [5, 7]. Huerta [8], who investigated the evolution of force components and specific energy under different working parameters during the grinding of glass, used diamond and SiC grains. He found that using SiC might induce viscous flow, whereas using diamond may cause fracture with localized flow.

Some of these investigations discussed the possibility of obtaining ductile streaks under certain conditions. It has been shown that if the depth of cut is lower than a certain critical depth, calculated with the undeformed chip thickness theory, ductile streaks could be obtained [5, 9–12]. For higher depth of cut, different damages can be generated. Zhong et al. [10, 13] observed three different damage regimes during the grinding of glass: ductile mode, brittle mode and mixed mode (ductile and fragile). In preliminary experiments of grinding of glass for building, in monograin configuration, two different damage regimes namely chipping and fragmentation were observed [14].

The wear of the wheel, especially the grains, influences the surface quality and the material removal mechanism. Indeed, Belkhira et al. [15] linked the roughness with the wear of abrasive grains. Luo et al. [16] enumerated different wears from the abrasive grains during the grinding of optical glass and showed the correlation between the glass surface quality and the wear of abrasive grains.

Grinding mechanism parameters have been studied by some authors. Huerta [8], for example, showed that grinding energies with SiC are about order of magnitude more than diamond. Takahashi and Funkenbusch [17] showed that if grains are damaged, the specific energy increases rapidly.

All these articles are about the grinding of glass for optical and ophthalmic applications (optical lens, infra-red, laser optics). The principal results are as follows:

- Possibility to obtain flow under some conditions;
- Nature of wheels bond and grains play an important role in this flow;
- Different damage regimes are observed: brittle, partial ductile and ductile;
- Relationship between grains wear and surface quality.

However, grinding of glass joint for building was not studied, and the relationship between the process and glass joint behaviour are not known.

In this article, we investigate the grinding of glass joint for different working parameters. The influence of these parameters and the specific energy on grounded glass is studied. Different observation tools and the multi-scale analysis were used to characterize the surface finish and differentiate the different damage regimes obtained during the arris edge process of glass joint.

2 Experimental Procedure

2.1 Devices Used: Specimen Type and Wheels Properties

All the grinding experiments of glass were performed on a CNC, Computer Numerically Controlled machine (VEC500 MIKRON). A dynamometric cell (Kistler device) relied to the acquisition system and fixed under the glass specimen which was supplied in rectangular block shape of size 400 × 100 × 10 mm was used for recording the normal (F_n) and tangential (F_t) force components. The grinding operation was carried out on only one edge of the specimen. Figure 1a shows a schematic illustration of the wheel and specimen configuration. A power cell is also available to record the active power during the grinding operation. The machine is equipped with a tank and a pump to inject the cutting liquid into the grinding zone.

A specified system installed on the tools ensures that cooling is maintained. This system follows the path of grinding. The working parameters during the grinding of glass are as follows: Wheel velocity (v_s), workpiece velocity (v_w) and depth of cut (a_p) as illustrated in Fig. 1a. The analysis will be limited to soda-lime silica glass (float

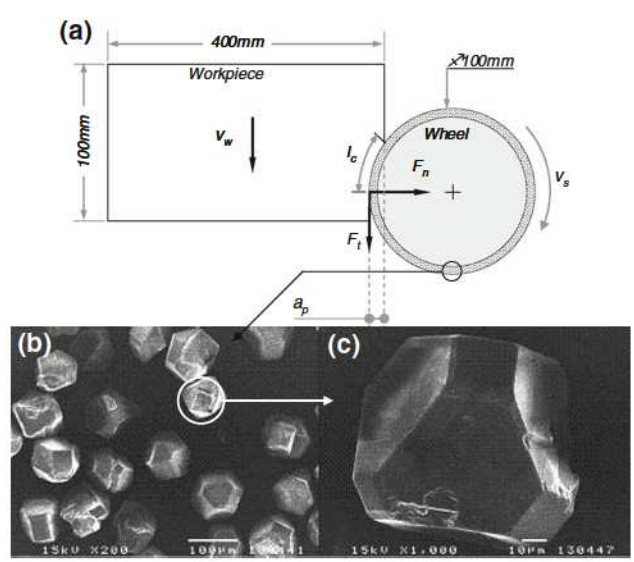

Fig. 1 Illustrations of (**a**) grinding parameters and micrographs of (**b**) regular diamond grains, (**c**) magnification of one diamond grains

Table 1 Characteristics of wheels used for experiments

Wheel type	Specification	Grain type	Grain size (μm)	Bond type	Concentration
Diamond-M	DC3 46N62.5M3	Diamond	46	Copper alloy	62.5

Table 2 Grinding parameters used for the different wheels

Wheel type	v_s (m s^{-1})	v_w (mm min^{-1})	a_p (mm)
Diamond-M	18, 20, 21, 22, 25, 27, 30, 35, 40	1,000, and 2,000	0.1

glass). The main components of soda-lime silica glass are: silica sand (73%), calcium oxide (9%), soda ash (13%), magnesium (4%) and various other materials added in very small quantity.

A wheel type with 100 mm diameter consisting of a diamond wheel with metal bond (Diamond-M) and regular grains with planar faces was considered for this study. Figure 1b and c showmicrographs of Diamond-M wheel grains and magnification of one grain, respectively. All characteristics of the grain are listed in Table 1.

In this work, the influence of the wheel velocities, the workpiece velocities and depth of cut were studied. During the experiments, semi-finishing configuration has been used. The manufacturer used wheel velocities ranging between 15 and 35 m s^{-1}, workpiece velocities between 1 and 5 m min^{-1} and maximum depth of cut of 0.5 mm. However, this depth of cut must be larger than the grains diameter.

We thus used 9 wheel velocities and 2 workpiece velocities for Diamond-N in the range given by the manufacturer. The CNC machine is limited to 2.5 m min^{-1} and Fillion [14] showed that there is an optimal workpiece velocity (1 m min^{-1}) for which efforts are weakest, which is why we used these two velocities. The depth of cut must be lower than 0.5 mm, but larger than the diameter of the grains. In addition, Huerta [8] showed that in general, an increase of the depth of cut (a_p) by a factor six does not produce noticeable differences in resulting surface morphology when grinding with diamond wheel. It is for these reasons that we chose only one value for depth of cut. All the parameter values are listed in Table 2. The tests were repeated five times for all conditions.

2.2 Multi-scale Surface Analysis

The analysis of the ground glass surfaces employed the multi-scale analysis. This entails the decomposition of topographic surfaces into different roughness scales. This decomposition uses continuous wavelet transform, which can be considered as a mathematical microscope, where the resolutions are the basic functions obtained from a single wavelet or mother wavelet ψ (x) by dilation (or compression) and translation [18]. The surface topography components pass through a filter bank which is a set of contracting wavelets. One defines the 2D wavelet transform of a 2D surface topography $f(x, y)$ by:

$$W_{b,a}(x,y)=\frac{1}{\sqrt{a_x a_y}}\int_{-\infty}^{+\infty} f(x,y)\psi\left(\frac{x-b_x}{a_x},\frac{y-b_y}{a_y}\right)\mathrm{d}x\mathrm{d}y \qquad (1)$$

where a_x, a_y are, respectively, the contraction coefficients according to the x and y directions, and b_x and b_y are the translation coefficients according to the x and y directions.

The "Mexican-hat-2D" wavelet is given by the following expression:

$$\psi(x,y) = (2-r)\exp(-r/2);\ r = x^2 + y^2 \qquad (2)$$

It is an isotropic wavelet, which admits good localization properties in the space field and the frequencies domain radially and symmetrically at the same time. It checks the conditions of existence well and exhibits filter band pass behaviours.

The various scales of the decomposition can be presented in a cube like stacking of images treated on a hierarchical basis of scales. The example in Fig. 2a and b show the 2D continuous wavelet decomposition of a topography generated by 32 scales.

The result of the decomposition makes it possible to identify the various scales after a 2D inverse wavelet transformation which is defined by:

$$f(x,y) = \frac{1}{C_g}\int_{-\infty}^{+\infty}\int_{-\infty}^{+\infty}\int_{-\infty}^{+\infty}\int_{-\infty}^{+\infty} W_{b,a}^{f}(x,y) \times \psi_{a,b}(x,y)\frac{\mathrm{d}b_x\mathrm{d}b_y\mathrm{d}a_x\mathrm{d}a_y}{a_x^2 a_y^2} \qquad (3)$$

where $C_g = \int_{-\infty}^{+\infty}\int_{-\infty}^{+\infty}\frac{|\psi(u,v)|^2}{uv}\mathrm{d}u\mathrm{d}v$. For Mexican Hat wavelet C_g is approximately equal to 3.541.

The methodology consists of extraction of each scale by inverse wavelet transform, and to quantify the arithmetic

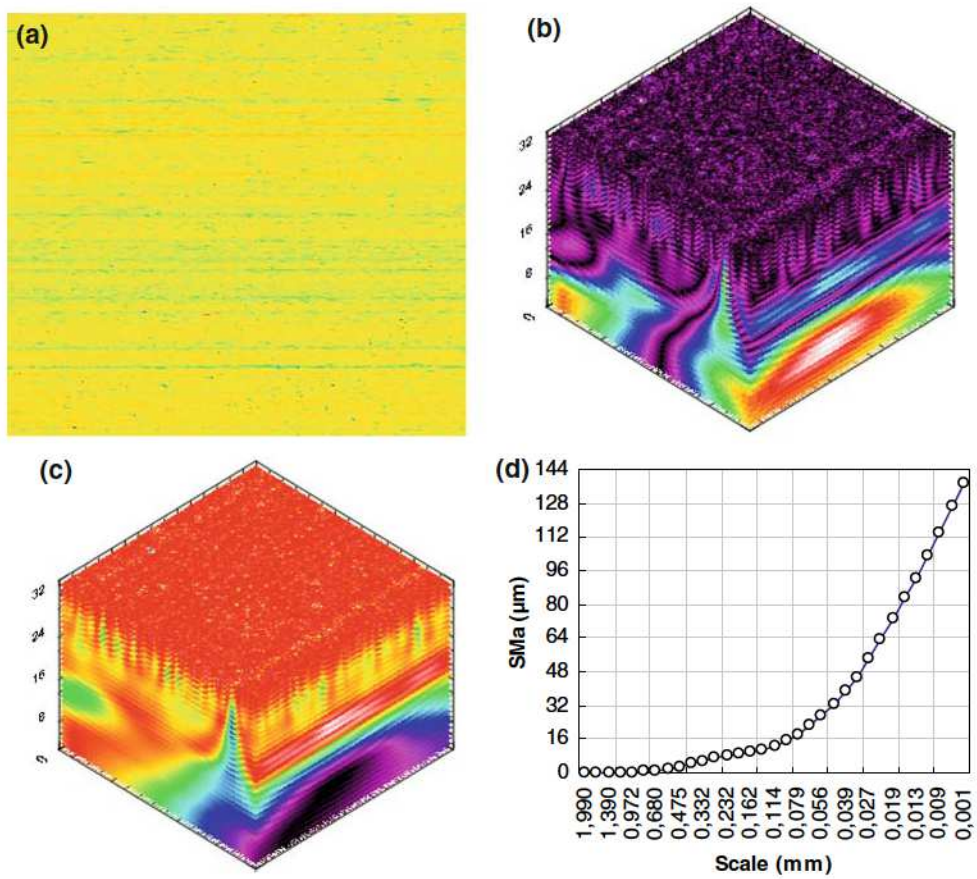

Fig. 2 Multi-scales decomposition of surface topography (**a**) ground glass surface, (**b**). wavelets transforms coefficients, (**c**) multi-scale decomposition of surface topography and (**d**) SMa spectrum

mean value for each scale. The objective is to determine the spectrum of arithmetic mean value from the scales of waviness to roughness SMa [19]:

$$\mathrm{SMa}(a) = \sum_{x=1}^{M}\sum_{y=1}^{N}\frac{\left|W_a^{*f}(x,y)\right|}{MN} \tag{4}$$

The main advantages of the wavelet transform over the existing signal processing techniques are its space frequency localization and multi-scale analysis of roughness and waviness.

Figure 2c and d show a multi-scale decomposition of ground surface topography and the determination of the SMa(a) spectrum, respectively. One can observe the decrease of roughness heights at each scale of decomposition, and the possibility to identify the manufacturing process signature in the SMa spectrum.

3 Results and Discussion

3.1 Grinding Regimes

Grinding regimes for brittle material involve different material removal mechanisms [2, 11–13, 17, 20]. Experimental findings proved the sensitivity of these mechanisms to the specific energy produced as a consequence of action of abrasive grains against the material during grinding. Tests conducted at various wheel and workpiece velocities show high dependence of the specific energy on grinding conditions. This dependence between the macro-mechanical responses and the grinding parameters results in three typical regimes. Those regimes can be distinguished from the evolution of the specific energy when the velocity varies from 18 to 40 m s^{-1} (cf. Fig. 3).

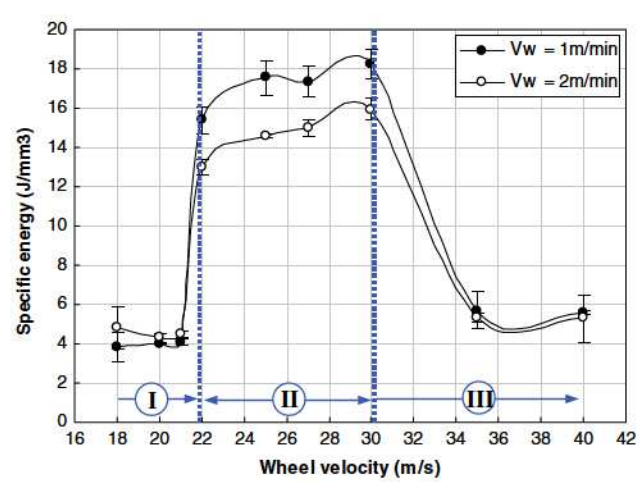

Fig. 3 Experimental specific energy versus wheel velocities

3.1.1 Specific Energy Evolution

A fundamental parameter for characterizing the grinding process is the specific energy, which is defined as the energy expended per unit volume of material removed. The specific grinding energy defines the mechanisms of releasing of a glass volume fraction from the operated workpiece. It is calculated from the following relationships:

$$u = \frac{P_m}{Q_w} \tag{5}$$

where P_m is the net grinding power (measured with power cell) and Q_w is the volumetric removal rate given by:

$$Q_w = v_w a_p b \tag{6}$$

where a_p is the depth of cut and b the thickness of the workpiece.

The evolution of specific energy with wheel velocity was studied for two workpiece velocities. The plot of this energy obtained with measured power is given in the Fig. 3. As one can see in the figure, the specific energy is weak (≈ 4 J mm^{-3} for $v_w = 1$ m min^{-1}) for the velocities under 22 m s^{-1}, but increases approximately by a factor 4 to reach 15 J mm^{-3}. From 22 to 30 m s^{-1}, the specific energy remains almost constant. Beyond the velocity of 30 m s^{-1}, the specific energy decreases steeply by a factor of 3 to reach approximately 5 J mm^{-3}. For the second workpiece velocity, the curve shows the same tendency, with an increase by a factor of 4 beyond 21 m s^{-1} and decrease by a factor of 3 beyond 30 m s^{-1}. It is also obvious in Fig. 3 that the specific energy decreases when the workpiece velocity increases. This decrease can be explained by the "size effect" theory [20], i.e. the energy increases with decreasing chip thickness. Indeed, when the uncut chip thickness (h_m) decreases the specific energy increases. This thickness is proportional to the workpiece velocity, and the increase in v_w increases h_m, therefore reducing the specific energy. The increase of specific energy at very low removal rates with small uncut chip thickness has been attributed to an increased tendency for ductile flow rather than fracture [21].

The behaviour of specific energy with respect to wheel velocity defines the different energy regimes. It is seen that there are three different regimes (I–III). The specific energy evolution is probably explained by different material removal mechanisms which will be described hereafter.

3.1.2 Grinding Forces

The evolution of the force with the wheel velocity was studied for two workpiece velocities. The plots of both, tangential and normal components are given in the Fig. 4. These plots show the zones of the different regimes. As for

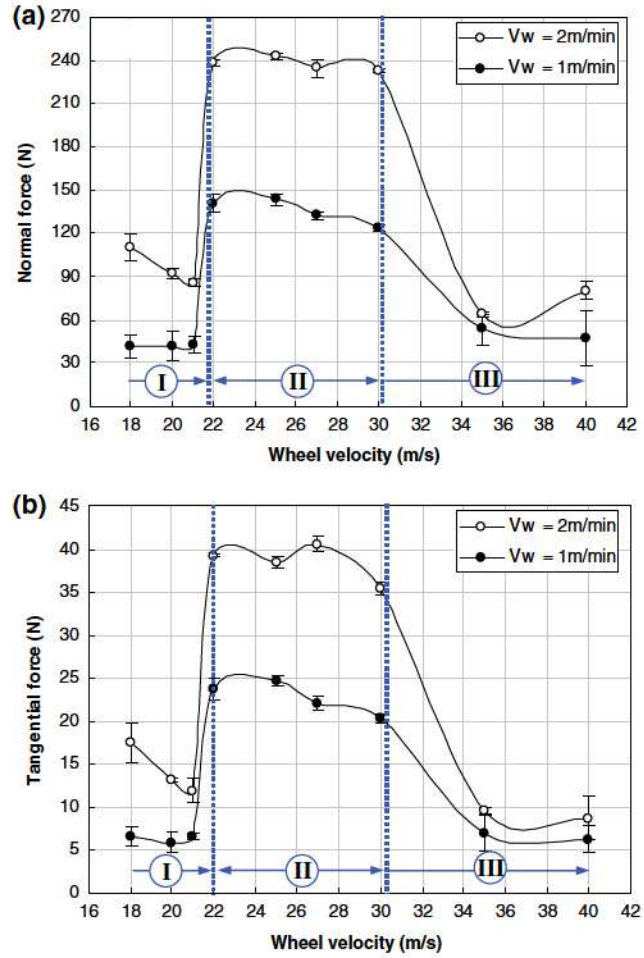

Fig. 4 Evolution of (a) normal component and (b) tangential component of force versus wheel velocities

the specific energy, the components of the force suddenly increase after 21 m s^{-1} and decrease beyond 30 m s^{-1}. In the regime I, the tangential and normal forces are low and increase suddenly by approximately a factor of 3 to reach regime II. In this regime, the forces are nearly constant, and beyond 30 m s^{-1} they decrease more slowly to attain regime III. In this transition, the forces decrease by a factor of 3 and 4, respectively, for v_w equal to 1 and 2 m s^{-1}. These variations are due to different material removal regimes as will be explained in a later section.

One can view that when the workpiece velocities increase, the force components increase. Indeed with this rise of workpiece velocity, the wheel-work contact lengths and grinding zone areas are also bigger. Thus the material removal rate per turn is higher and a greater force is needed to remove the material.

In order to justify and characterize these three regimes, some observations with scanning electron microscopy (SEM) and multi-scale analysis were carried out. The first method was used to observe the damage on the ground

surface, and the last was performed to study the different scales of the surface signature (roughness, waviness which corresponds to streak generation and form defect).

3.2 Material Removal Mechanisms: Damage

3.2.1 SEM Observations

We present here different SEM micrographs of ground surfaces to characterize the three regimes. Figure 5a shows regime I, and Fig. 5b is an enlarged view of one part of the observed surface. Figure 5c and d (enlarged view) illustrate regime II and Fig. 5e and f display regime III.

The first regime is characterized by brittle fracture (cracks and chip). One can see in Fig. 5b, an enlarged view of Fig. 5a, some chip. Twist hackle marks [22] are clearly visible. This suggests that the fracture pattern is driven mainly in mode I combined with a weak mode III component. The river line patterns indicate the direction of propagation of the crack. These lines are approximately equally spaced (≈ 1 µm), which is in good agreement with the literature results [23]. Regime III is quite different. Some cracks are visible, in Fig. 5e and f but less than in regime I. The particularity of this regime is the fact that some displaced materials (black arrow) are visible. Following Venkatesh et al. [5], two partial ductile regimes can be identified: one with cutting action accompanied by chip formation (regime I) and one by ploughing action with displaced material (regime III). Regime II is characterized by debris. The surfaces are less smooth. The cracks are more visible, bigger and more numerous than the other regimes. The material is removed by microcracking and corresponds to typical "abrasion" operations [24].

The above observations showed different damage surfaces clearly. However, we cannot conclude on the observed damage mode. That is why the multi-scale surface analysis is used.

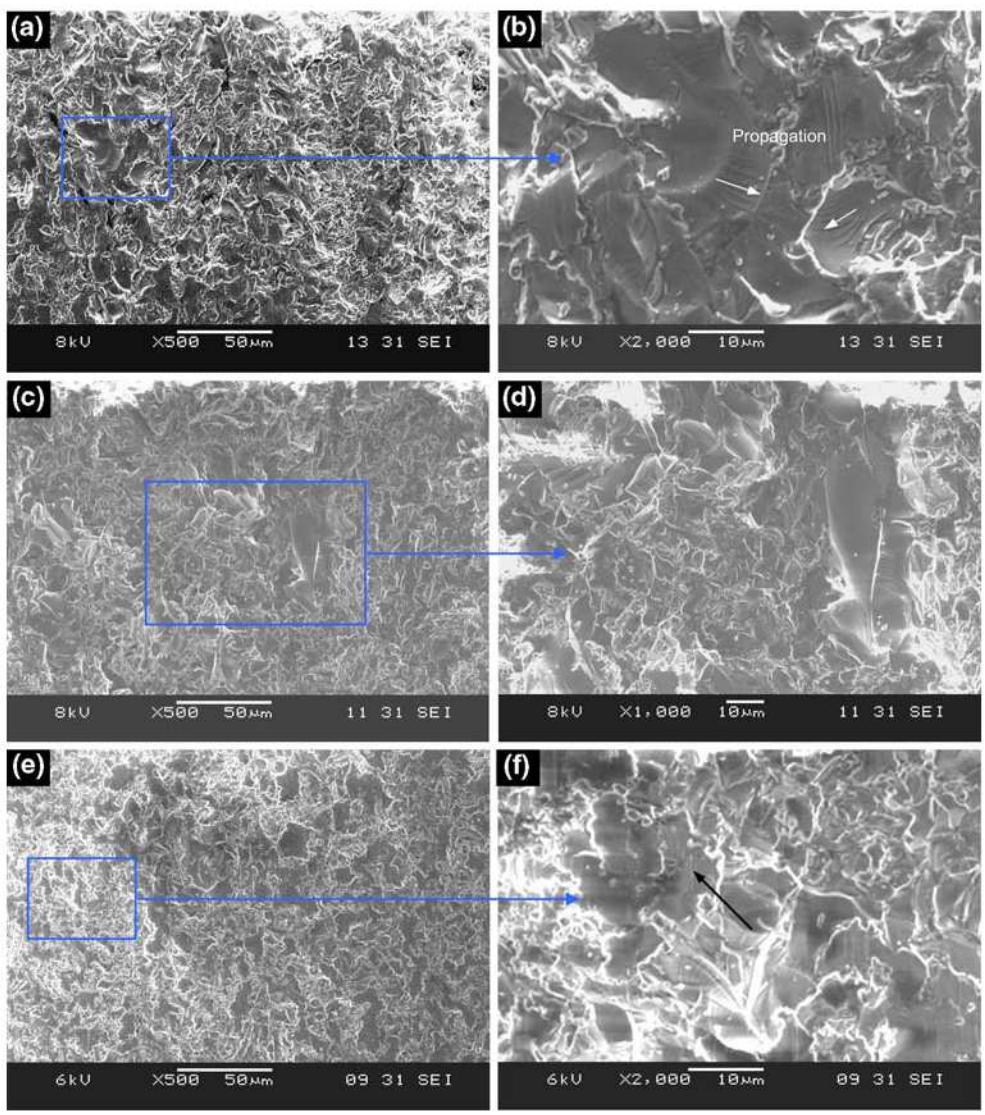

Fig. 5 SEM micrographs of ground surfaces obtained for (**a**, **b**) regime I ($v_s = 20$ m s^{-1}), (**c**, **d**) regime II ($v_s = 25$ m s^{-1}), (**e**, **f**) regime III ($v_s = 40$ m s^{-1}). (**b**, **d**, and **f**) are enlargement view of (**a**, **c**, **e**), respectively

3.2.2 Multi-scale Surface Analysis

A simple value of arithmetic roughness (R_a) is not enough for characterizing precisely the surface state of the glass edge acquired after grinding because the topography of the surface is changed on a broad band of wavelength. A fine analysis is therefore necessary to separate the changed scales. That is why we used the multi-scale technique to obtain the signature of the different ground surfaces. Characterization of the surface topography of glass edge was carried out by a three dimensional white light interferometer (Wyko NT 3300). The surface was sampled in 320 × 1,546 points with a 3.88 μm step scale in the x-direction and in the y-direction which correspond to a surface of 1.24 × 6 mm.

Figure 6 shows the SMa spectrum on its various scales for three wheel velocities (one per regime) used during the grinding of the glass. One can see three different zones corresponding to the different roughness scales. The right zone linked to high frequencies corresponds to roughness. The central zone is related to the waviness which is the amplitude of the streaks for our study. Finally, the left zone results in form defects induced by the grinding wheel. For the low and high wheel velocities ($v_s = 18$, 21, 35, 40 m s^{-1}), we can see a peak in the waviness zone which corresponds to streaks localized on a 0.85 mm scale. These peaks justify the presence of flow. In regime I and III, there is simultaneous ductile flow and brittle fracture (chip and cracks), whereas, for the intermediary wheel velocities ($v_s = 22$, 25, 27 and 30 m s^{-1}), there is no peak in the waviness zone which proves the absence of streaks and thus only brittle fracture.

In the right zone we can see that for the middle velocities the SMa is constant with a mean value of 0.15 μm, while for the low and high velocities the spectrum of the mean arithmetic varies between 0.15 and 0.3 μm. Therefore, the roughness obtained on glass surface for intermediary velocities is better than that acquired with low and high velocities. We can also point out that for the low and high wheel velocities the form defects are more important (peak in shape scale) than for surfaces ground with intermediate velocities.

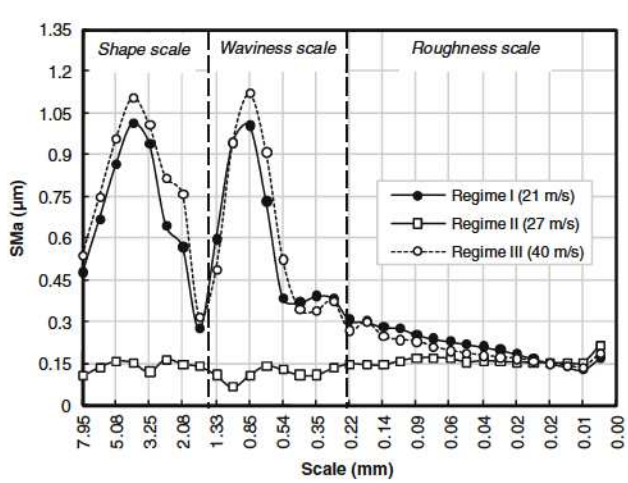

Fig. 6 Evolution of the SMa spectrum versus scale. Signature of the wheel on ground surface with different wheel velocities. Identification of the different scales

Therefore, we can so conclude that for intermediary wheel velocities the roughness is weaker than for other velocities but the wheel does not generate streaks. This can result in weaker mechanical resistance, owed especially to the presence of cracks (big and more numerous).

From this multi-scale analysis, we can conclude there is presence of streaks for the low and high wheel velocities and better roughness for the intermediary velocities.

3.2.3 Discussion

From observations of the SEM micrographs, we saw three different brittle fracture regimes and the multi-scale analysis verified whether streaks, which are characteristic of ductile mode were present. The three regimes observed with the analysis of specific energy refer therefore, to three different material removal regimes. These mechanisms are as follows:

- Regime I: partial ductile grinding associated with ductile streak and brittle fracture;
- Regime II: corresponds to the fragmentation (crushing) grinding mechanisms;
- Regime III: corresponds to the partial ductile grinding.

As mentioned above, regime I and III are quite different. One is partial ductile with cutting action accompanied by chip formation (regime I) and one by ploughing action with displaced material (regime III). In regime II, the glass is crushed (or shattered). For regime I and III, the specific energy and force components are low, whereas for the second regime, they are high. The transition of the different regimes is thus obtained when the specific energy increase, which is proportional to the grinding force. Swain [24] who used the single grit apparatus, observed this material removing mechanism: plastic grooving, generation of cracks and chip and crushing. He found that these mechanisms are directly related to the force on the abrasive grain with higher force corresponding to an increase in the observed surface fracture. Single grain abrasive experiments on glass [25] also showed similar transition in the material remove process. Fillion [14], in single grain experiments in grinding condition, saw the fragmentation and chipping regime. The first one was obtained for larger forces. Le Houérou et al. [26] observed three regimes during the scratch of glass with a Vickers indenter under

increasing loading cycle: the first one was the micro ductile regime, the second was the micro cracking characterized by cracks and chips and the third one was the micro-abrasive regime and gave rise to many debris with occasional cracks.

The wheel velocity also played a small part in the material removal process. For the low velocities, the first regime took place. For the intermediary velocities (22–30 m s^{-1}), the second regime appeared and beyond 30 m s^{-1} the third regime appeared. In regime II, the material was removed by microcracking with the presence of median cracks which corresponds to a typical "abrasion" operation [24]. This trend might explain the increase of the force components. The transition between regime II and III can be explained by the underformed chip thickness (h_m) (or maximum depth of cut) which decreases when wheel velocities increase. With smaller values of h_m, the forces might be lower. At higher wheel velocities the contact pressure reduced, leading to lower forces. Thus, the severity of the cutting process seems to decrease [27].

3.3 Friction in Glass Shaping

The evolution of the normal force with the tangential force was studied for the two workpiece velocities in dry and lubricated conditions. Figure 7 presents this evolution. One can see linear relationships between the normal and tangential forces for the dry and lubricated cases. Such linear relations have also been obtained for the metallic materials [20]. Malkin [20] divided the force into cutting and sliding components:

$$F_t = T_{t,c} + F_{t,sl} \text{ and } F_n = T_{n,c} + F_{n,sl} \tag{7}$$

where $F_{n,c}$ and $F_{t,c}$ are the normal and tangential forces for cutting and $F_{n,sl}$ and $F_{t,sl}$ are those for sliding. After having observed the proportionality between forces and wear-flat area, which implies a constant average contact pressure and

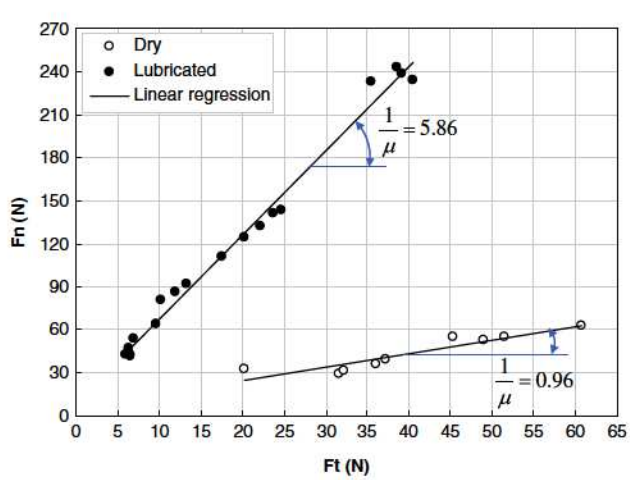

Fig. 7 Evolution of normal component versus tangential component

friction coefficient (μ) between the wear flats and the workpiece, the following relationship between normal and tangential forces was proposed [20]:

$$F_n = \frac{1}{\mu} F_t + \frac{\mu F_{n,c} - F_{t,c}}{\mu} \tag{8}$$

where μ is the friction coefficient given by the following relationship:

$$\mu = \frac{F_{t,sl}}{F_{n,sl}} \tag{9}$$

This situation is envisioned for flat grains which is the case for our study (Fig. 1b, c). According to Eq. 8, the slope of this linear relation corresponds to $1/\mu$. The friction coefficient is thus 0.17 and 1.04, respectively, for the lubricated and dry case. This linear relation suggests also linearity between the flat grains and the forces.

In the dry condition, the friction coefficient is larger than in the lubricated case. The role of the lubricant is to cool the process and decrease the friction coefficient. This role does not explain the large difference. There are probably different material removal mechanisms. The specific energy in dry and wet conditions was therefore studied. Figure 8a display this energy for the two cases at one workpiece velocity. Micrographs and the profile of the ground surface in dry condition are presented in Fig. 8b and c, respectively.

The specific energy in the dry condition is larger than that in the lubricated condition as one can see in the range of 20–30 m s^{-1} in Fig. 8a. The two plots show the same behaviour i.e. sudden increase in specific energy after the velocity of 21 m s^{-1} after which it remains nearly constant. The micrograph of ground surface at 25 m s^{-1} shows a succession of scratches (Fig. 8b). The succession of dark and clear lines in Fig. 8b is due to the difference of depth between the top and the bottom of the groove. These scratches are justified by the profile of the surface (Fig. 8c). The width of the plastic groove is 1 mm and the depth is about 66 µm. These scratches are also equally spaced. The temperature at the grounded glass surface during the grinding in dry condition is high enough to soften the glass. Consequently, the material exhibits melt state in such a manner that the glass is pushed locally under the action of the wheel: it is a ploughing regime. For lubricated condition, the surface is crushed (Fig. 5c, d) as explained above (regime II: crushing).

It is also clear that the difference in specific energy for these two conditions can be explained by different material removal mechanisms. The ploughing mechanism in dry condition explains the increase in specific energy and thus the higher friction coefficient than in lubricated condition. One can also view some cracks at the bottom of groove (white arrow). This damage is known as thermal cracks.

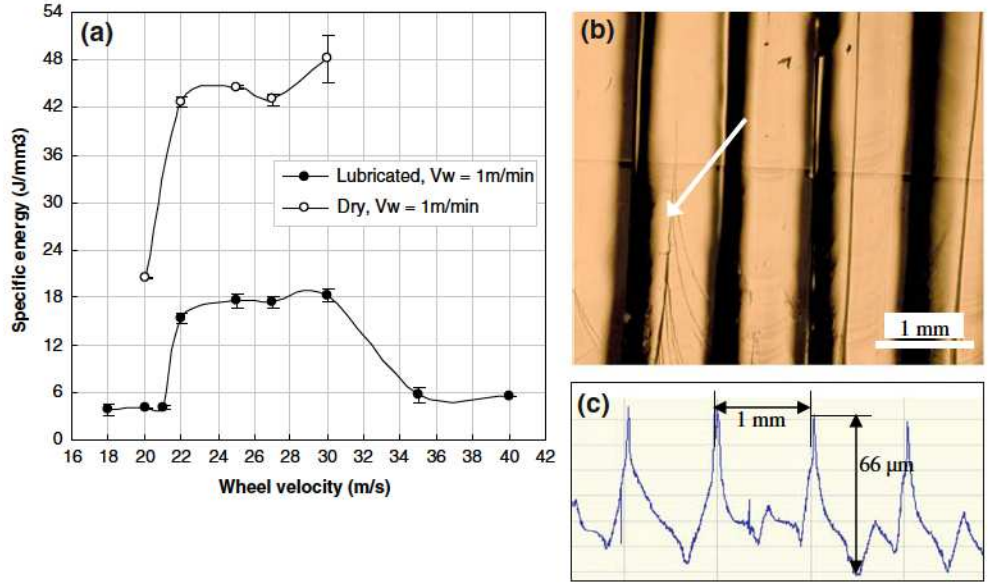

Fig. 8 Evolution of specific energy versus wheel velocity for lubricated and dry conditions (**a**), micrograph of ground surfaces on dry condition (**b**) and his profile (**c**) for velocity 25 m s^{-1}

4 Conclusions

Glass shaping which corresponds to the removal of the edges with a wheel was investigated. This glass grinding was realized for different wheel and workpiece velocities. The study of the specific energy displays three different energy regimes. In combination with the investigation of specific energy, SEM micrographs and multi-scale surface analysis enabled us to show three different damage regimes which are as follows:

- Regime I: partial ductile with cutting action accompanied by chip formation;
- Regime II: crushing or fragmentation regime;
- Regime III: partial ductile by ploughing action with the displaced material.

In the first one, there are streaks with brittle fracture, especially chips, in which one can clearly see the well known twist hackle mark. In Regime II, the glass surfaces are crushed and much debris is present. In the last regime, streaks, displaced material and some cracks are visible. The analysis of surface finish with the multi-scale technique shows different trends. In Regimes I and III, the wheel generates streaks and forms defects which are visible in the SMa spectrum (peaks in the waviness and form defect scale), whereas the roughness obtained in the regime II is weaker than in the two other regimes. In this crushed regime, the mechanical strength is probably weaker due to the cracks which are bigger and more numerous.

The evolution of force components shows a similar tendency for the grinding of metals. Indeed, we obtained linear relationships between the tangential and normal forces which suggests proportionality between the forces and flat grain area. This implies a constant average contact pressure and friction coefficient between flat grains and the workpiece. The friction coefficient obtained in the dry condition is larger than in the wet condition, which is explained by a different material removal mechanism. In the dry condition, the material is "pushed": ploughing regime, whereas in wet condition, the material is crushed: crushing regime.

Acknowledgements The authors gratefully acknowledge the technical support of *Saint-Gobain Glass* Company.

References

1. Bowden, F.P., Hughes, T.P.: Physical properties of surfaces–IV. Polishing, surface flow and the formation of the Beilby layer. Proc. R. Soc. Lond. **A160**, 575–587 (1937)
2. Bowden, F.P., Scott, H.G.: The polishing, surface flow and wear of diamond and glass. Proc. R. Soc. Lond. **A248**, 368–378 (1958)
3. Fielden, J.H., Rubenstein, C.: The grinding of glass by a fixed abrasive. Glass Technol. **10**, 73–83 (1969)
4. Bridgman, P.W., Simon, I.: Effects of very high pressures on glass. J. Appl. Phys. **24**, 405–413 (1953)
5. Venkatesh, V.C., Izman, S., Vichare, P.S., Mon, T.T., Murugan, S.: The novel bondless wheel, spherical glass chips and a new method of aspheric generation. J. Mater. Process. Technol. **167**, 184–190 (2005)
6. Sun, X., Stephenson, D.J., Ohnishi, O., Baldwin, A.: An investigation into parallel and cross grinding of BK7 glass. Prec. Eng. **30**, 145–153 (2006)
7. Desmars, Y., Margerand, S.: Rappel sur le façonnage du verre. Rapport technique. Centre de Développement Industriel Saint-Gobain Glass Thourotte (1994)
8. Huerta, M.: Grinding of glass and effects on surface structure and fracture strength. Ph.D., The University of Texas at Austin (1974)
9. Fang, F.Z., Liu X.D., Lee, L.C.: Micro-machining of optical glasses – a review of diamond-cutting glasses. Sadhana **28**, 945–955 (2003)
10. Zhong, Z.: Ductile or partial ductile mode machining of brittle materials. Int. J. Adv. Manuf. Technol. **21**, 579–585 (2003)

11. Bifano, T.G., Dow T.A., Scattergood, R.O.: Ductile regime grinding: a new technology of machining brittle materials. ASME J. Eng. Indust. **113**, 184–189 (1991)
12. Ngoi, B.K.A., Sreejith, P.S.: Ductile regime finish machining – a review. Int. J. Adv. Manuf. Technol. **16**, 547–550 (2000)
13. Zhong, Z.: Partial-ductile grinding, lapping and polishing of aspheric and spherical surfaces on glass. Mater. Manuf. Process. **12**, 1063–1073 (1997)
14. Fillion, E.: Etude du procédé de façonnage verrier. Rapport de projet de recherche, LMPF-ENSAM (2006)
15. Belkhira, N., Bouzida, D., Herold, V.: Correlation between the surface quality and the abrasive grains wear in optical glass lapping. Tribol. Int. **40**, 498–502 (2007)
16. Luo, S.Y., Tsai, Y.Y., Chena, C.H.: Studies on cut-off grinding of BK7 optical glass using thin diamond wheels. J. Mater. Process. Technol. **173**, 321–329 (2006)
17. Takahashi, T., Funkenbusch, P.D.: Micromechanics of diamond composite tools during grinding of glass. Mat. Sci. Eng. **A285**, 69–79 (2000)
18. Zahouani, H., Lee, S.H., Vargiolu, R., Rousseau, J.: Characterization of surface topography by continuous wavelet transform. Acta Phys. Superficierum **IV**, 1–23 (2001)
19. Zahouani, H., Mezghani, S., Vargiolu, R., Dursapt, M.: Identification of manufacturing signature by 2D wavelet decomposition. Wear **264**, 480–485 (2008)
20. Malkin, S.: Grinding Technology: Theory and Applications of Machining with Abrasives. Society of Manufacturing Engineers, Dearborn, Michigan (1989)
21. Hwang, T.W., Evans, C.J., Malkin, S.: Size effect for specific energy in grinding of silicon nitride. Wear **225–229**, 862–867(1999)
22. Standard practice for interpreting glass fracture surface features, in C 1256-93 (reapproved 2003). ASTM International (1993)
23. Hull, D.: Fractography: Observing Measuring and Interpreting Fracture Surface Topography. Cambridge University Press, Cambridge (1999)
24. Swain, M.V.: Microfracture about scratches in brittle solids. Proc. R. Soc. Lond. **A336**, 575–597 (1979)
25. Molloy, P., Schinker, M.G., Doll, W.: Brittle fracture mechanisms in single point glass abrasion. International Technical Symposium on Optical and Electro-optical: Applied Science and Engineering (SPIE, vol. 802). The Hague, NL (1987)
26. Le Houérou, V., Sangleboeuf, J.-C., Dériano, S., Rouxel, T., Duisit, G.: Surface damage of soda-lime-silica glasses: indentation scratch behaviour. J. Non-Cryst. Solids **316**, 54–63 (2003)
27. Hwang, T.W., Evans, C.J., Malkin, S.: High speed grinding of silicon nitride with electroplated diamond wheels, Part 2: wheel topography and grinding mechanisms. ASME J. Manuf. Sci. Eng. **122**, 42–50 (2000)